Hindawi Publishing Corporation
International Journal of Photoenergy
Volume 2014, Article ID 342132, 7 pages
http://dx.doi.org/10.1155/2014/342132

Research Article

Electronic Structure and Optical Properties of N/Si-Codoped Anatase TiO_2 Evaluated Using First Principles Calculations

Huey-Jiuan Lin[1] and Hsuan-Chung Wu[2,3]

[1] *Department of Materials Science and Engineering, National United University, Miaoli 36003, Taiwan*
[2] *Department of Materials Engineering, Ming Chi University of Technology, New Taipei 24301, Taiwan*
[3] *Center for Thin Film Technologies and Applications, Ming Chi University of Technology, New Taipei 24301, Taiwan*

Correspondence should be addressed to Hsuan-Chung Wu; hcwu@mail.mcut.edu.tw

Received 13 November 2013; Revised 9 February 2014; Accepted 3 March 2014; Published 27 April 2014

Academic Editor: Pramod H. Borse

First principles calculations were used to evaluate the electronic structure and optical properties of N/Si-monodoped and N/Si-codoped TiO_2 to further understand their photocatalytic mechanisms. In accordance with the atomic distance between N and Si dopants, this study considered three N/Si codoping configurations, in which the N dopant had a tendency to bond with the Si dopant. The calculations showed that the bandgaps of the N/Si codoping models were narrow, in the range 3.01–3.05 eV, redshifting the intrinsic absorption edge. The Si 3*p* orbital of N/Si-codoped TiO_2 plays a key role in widening the valence band (VB), thereby increasing carrier mobility. In addition, the N-induced impurity energy level in the forbidden band appears in all three N/Si codoping models, strengthening absorption in the visible region. The bandgap narrowing, VB widening, and impurity energy levels in the forbidden band are beneficial for improving the photocatalytic activity of N/Si-codoped TiO_2.

1. Introduction

Since the pioneering work of Fujishima and Honda in 1972 [1], titanium dioxide (TiO_2) has been widely studied as a promising photocatalytic material because of its excellent properties (e.g., it is nontoxic, inexpensive, and chemically stable). However, pure anatase TiO_2 has a wide bandgap of 3.2 eV and only absorbs in the UV region (~5%) of solar energy. Therefore, its solar energy use is restricted. Much research has recently been devoted to developing methods of extending the optical absorption of TiO_2-based materials into the visible region.

Doping TiO_2 with various dopants including transition metals such as Mo [2], Co [3], and Au [4] and nonmetals such as N [5–9], Si [10–14], P [15], and S [16] is a popular method of enhancing the characteristics of TiO_2. Since the report of Asahi et al. in 2001 [5], N has been considered the most effective nonmetallic elemental dopant and has been studied further [5–9]. Doping with Si is also effective for enhancing the photocatalytic activity of TiO_2 [10–14]. Doping TiO_2 with two dopants (i.e., codoping) has recently been developed as a method to enhance photocatalytic activity, and promising results have been reported for codoping TiO_2 with nitrogen and silicon (N/Si) [17–19]. Ozaki et al. [17, 18] fabricated nitrogen-doped silica-modified TiO_2, which showed strong absorption in the 400–500 nm visible region and exhibited high photocatalytic activity toward visible-light-induced acetaldehyde decomposition. They indicated that the amount of Si added significantly increased the amount of N and the visible-light-induced photocatalytic activity. Hou et al. [19] found that N-doped SiO_2/TiO_2 exhibited higher photocatalytic activity than N-doped TiO_2 when the weight ratio of SiO_2/TiO_2 was in the range 0.05–0.20. Shi et al. [20] performed first principles calculations to evaluate the energies and electronic properties of N/Si-codoped TiO_2. The calculated energies indicated that Si doping increases the concentration of N in N/Si-codoped TiO_2. The bandgap of Si/N-codoped TiO_2 was significantly narrowed to 1.63 eV. However, the calculated bandgap of pure anatase TiO_2 (2.18 eV) was underestimated owing to the limitations of standard

density functional theory (DFT). A few approaches such as DFT + U (Hubbard U) and hybrid functionals have been used to investigate TiO_2-based materials in order to overcome this limitation. Long and English [21] used Heyd-Scuseria-Ernzerhof (HSE06) hybrid DFT calculations to investigate the effects of N/Si codoping on the electronic properties of anatase TiO_2. Their calculated bandgap of anatase TiO_2 was 3.2 eV, which was consistent with the experimentally obtained bandgaps. The calculated results suggest that double-hole coupling plays a key role in ensuring high photocatalytic activity in the visible region for TiO_2-based photocatalysts.

The DFT + U is a method of correcting the underestimation of the bandgap and involves adding an orbital-dependent term to the DFT potential; it has previously been used to describe the electronic structures of transition-metal oxides [22–25]. Thus, we used the DFT + U method to more accurately represent the electronic structure and optical properties of N/Si-codoped TiO_2. The N/Si codoping system included three N-Si-distance-based models, which were compared with the N-monodoped, Si-monodoped, and pure TiO_2 models to further understand the mechanism of N/Si-codoping-induced photocatalytic activity enhancement. The optimized structures and Mulliken charges of the N-, Si-, and N/Si-doped TiO_2 were also analyzed and compared with corresponding values in the literature.

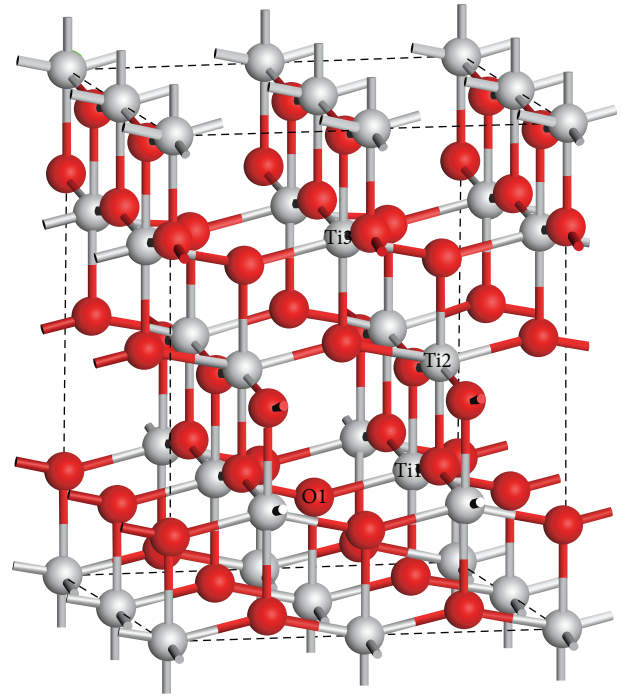

Figure 1: Structural model for pure anatase TiO_2 and doping sites. Red and gray spheres represent O and Ti atoms, respectively.

2. Calculation Models and Methods

Figure 1 shows the $2 \times 2 \times 1$ 48-atom anatase TiO_2 supercell model considered in this study. The N-monodoping and Si-monodoping models were constructed by substituting one O atom (from the O1 site) with one N atom ($N_{s(O)}$ model) and substituting one Ti atom (from the Ti1 site) with one Si atom ($Si_{s(Ti)}$ model), respectively. The corresponding concentrations of N and Si were both 2.08 at.% (dopant atoms/total atoms). In addition, we considered three N/Si codoping configurations in which the O1 atom was substituted with one N atom. The Ti1, Ti2, or Ti3 sites were substituted with one Si atom in the N/Si-1, N/Si-2, or N/Si-3 models, respectively. Our calculations showed that the enthalpy of the N/Si-1 model was the lowest (−37865.04 eV), indicating that the N/Si-1 structure was more stable than the N/Si-2 (−37864.71 eV) and N/Si-3 (−37864.73 eV) ones. This implies that the Si in the N/Si codoping model tends to bond with the N (forming Ti-N-Si bonds), which is consistent with the formation energy calculation results in the literature [20].

CASTEP software was used to perform the first principles calculations [26]. The potentials of ion core and valence electrons were modeled using ultrasoft pseudopotentials in the Vanderbilt form [27]. The valence electron configurations of the atoms were $2s^2 2p^3$ for N, $2s^2 2p^4$ for O, $3s^2 3p^2$ for Si, and $3s^2 3p^6 3d^2 4s^2$ for Ti. The wave functions of the valence electrons were expanded through a plane-wave basis set, and the cut-off energy was set to 400 eV. The Monkhorst-Pack-scheme-based K-point grid sampling was set at $4 \times 4 \times 3$ (i.e., $<0.04\ \text{Å}^{-1}$) [28]. The convergence threshold for self-consistent iterations was set to 1×10^{-6} eV. The optimization parameters were set as follows: energy change = 1×10^{-5} eV/atom, maximum force = 0.03 eV/Å, maximum stress = 0.05 GPa, and maximum displacement tolerance = 0.001 Å.

We previously used the DFT + U method and the following formalism to describe the exchange and correlation potential [6, 24]:

$$E_{\text{DFT+U}} = E_{\text{DFT}} + \frac{\text{U} - J}{2} \sum_{\sigma} \text{Tr}\left[\rho^{\sigma} - \rho^{\sigma}\rho^{\sigma}\right], \quad (1)$$

where ρ^{σ} denotes the spin (σ)-polarized on-site density matrix. The spherically averaged Hubbard parameter, U, describes the increase in energy caused by placing an extra electron at a particular site, and the parameter J (1 eV) represents the screened exchange energy. The effective Hubbard parameter, $\text{U}_{\text{eff}} = \text{U} - J$, accounts for the on-site Coulomb repulsion for each affected orbital. Here, the effective on-site Coulomb interaction is $\text{U}_{\text{eff}} = 8.4$ eV for Ti $3d$ in the DFT + U approach (see Figure S1 in Supplementary Material available online at http://dx.doi.org/10.1155/2014/342132).

3. Results and Discussion

3.1. Structural Optimization. Table 1 summarizes the average optimized bond length and the volume difference ratios of all the doping models and the pure anatase TiO_2. In the pure anatase TiO_2, each Ti atom is horizontally and vertically surrounded by four and two adjacent O atoms, respectively; the average length of the Ti–O bond is 1.992 Å. When an O atom is substituted with one N atom ($N_{s(O)}$ model), the Ti–O (1.994 Å) and Ti–N (2.045 Å) bonds were longer than the Ti–O bond in the pure TiO_2, expanding the volume. Because

Table 1: Average optimized bond length and volume difference ratio for N/Si-doped TiO_2.

Models	Bond length (Å)				Volume difference ratio (%)
	Ti–O	Ti–N	Si–O	Si–N	
Anatase TiO_2	1.992	—	—	—	—
$N_{s(O)}$	1.994	2.045	—	—	0.4
$Si_{s(Ti)}$	1.990	—	1.828	—	−2.0
NSi-1	1.991	2.099	1.818	1.894	−1.5
NSi-2	1.992	2.042	1.830	—	−1.5
NSi-3	1.992	2.042	1.830	—	−1.5

Table 2: Mulliken atomic population and bond population for N/Si-doped TiO_2.

Model	Atomic population (|e|)				Bond population (|e|)			
	Ti	O	N	Si	Ti–O	Ti–N	Si–O	Si–N
Anatase TiO_2	1.48	−0.74	—	—	0.343	—	—	—
$N_{s(O)}$	1.47	−0.74	−0.60	—	0.345	0.337		—
$Si_{s(Ti)}$	1.50	−0.76	—	1.77	0.342	—	0.410	—
NSi-1	1.49	−0.76	−0.68	1.74	0.343	0.335	0.402	0.500
NSi-2	1.49	−0.76	−0.60	1.77	0.343	0.333	0.408	—
NSi-3	1.49	−0.76	−0.60	1.77	0.342	0.333	0.407	—

the ionic radius and electronegativity of N (1.71 Å for N^{3-} and 3.04) are larger and smaller than those of O (1.32 Å for O^{2-} and 3.44) [29, 30], respectively, the Ti–N bond is longer than the Ti–O one in the $N_{s(O)}$ model [6]. Conversely, the Ti–O and Si–O bonds in the $Si_{s(Ti)}$ model are both shorter than the Ti–O bond in the pure anatase TiO_2, thereby shrinking the lattice because the Si^{4+} radius and Si electronegativity (0.40 Å for Si^{4+} and 1.90) are smaller and higher than those of Ti^{4+} and Ti (0.61 Å for Ti^{4+} and 1.54) [30, 31], respectively. This result is consistent with the previously obtained experimental results [10, 11] and theoretical calculations [20].

In the N/Si-2 and N/Si-3 models, the N-Si distance is longer, weakening the atomic interactions between the N and Si atoms. Therefore, the Ti–N and Si–O bond lengths in the N/Si-2 and N/Si-3 models are closer to those in the monodoping models ($N_{s(O)}$ and $Si_{s(Ti)}$). In the N/Si-1 model, the bond lengths vary in descending order as follows: Ti–N > Ti–O > Si–N > Si–O. The Ti–N bond in the N/Si-1 model (2.099 Å) is longer than that in the N/Si-2 and N/Si-3 models (both = 2.042 Å); the Si–O bond in the N/Si-1 model (1.818 Å) is shorter than that in the N/Si-2 and N/Si-3 models (both = 1.830 Å). Consequently, the volume difference ratios of these three codoping models are almost identical (−1.5%) and are between those of the $N_{s(O)}$ (0.4%) and $Si_{s(Ti)}$ (−2.0%) models.

3.2. Mulliken Population. Table 2 summarizes the average Mulliken atomic and bond populations of each N/Si model. The average atomic populations of the Ti and O atoms in the pure anatase TiO_2 are 1.48 and −0.74 |e|, respectively, suggesting that the Ti atoms tend to lose electrons and the O atoms tend to gain them. The Mulliken population of N atoms (−0.60 |e|) is larger than that of O atoms (−0.74 |e|) in the $N_{s(O)}$ model because of the former's smaller electronegativity. The atomic population of Si atoms (1.77 |e|) is larger than that of Ti atoms (1.50 |e|) in the $Si_{s(Ti)}$ model, indicating that Si atoms transfer more electrons to the surrounding O atoms thereby reducing the average atomic population of O atoms.

The atomic population of Si atoms (1.74 |e|) in the N/Si-1 model is slightly smaller than that of those in the $Si_{s(Ti)}$ model because N atoms are less electronegative than O atoms. Further, the atomic population of N atoms in the N/Si-1 model (−0.68 |e|) is smaller than that of N atoms in the N/Si-2 and N/Si-3 models (−0.60 |e|), suggesting that N atoms can gain more electrons from the Si atoms in the N/Si-1 model because the N atoms are directly bonded to the Si atoms. The atomic populations of N atoms (−0.60 |e|) in the N/Si-2 and N/Si-3 models are the same as those in the $N_{s(O)}$ model, implying that there is, again, almost no interaction between N and Si atoms in the N/Si-2 and N/Si-3 models.

The Ti–O bond population was larger than the Ti–N one, indicating that Ti–O bonds are more covalent than Ti–N ones. Further, the Si–N and Si–O bond populations in each model are in the range 0.402–0.500 |e|, meaning that Si–N and Si–O bonds were more covalent than the Ti–N and Ti–O ones.

3.3. Electronic Structure. Figure 2 shows the band structures calculated for the N/Si-monodoped and codoped TiO_2 models. The Fermi level, indicated by the dotted line, was set to zero. The bandgap obtained for the pure anatase TiO_2 was 3.21 eV, as shown in Figure 2(a), and is consistent with experimentally obtained bandgaps. The bandgap in the $N_{s(O)}$ model (Figure 2(b)) was 3.09 eV, which was less than that of the pure anatase TiO_2. An isolated impurity energy level resulting from the empty N-2*p* orbital above the valence band maximum (VBM) at 1.44 eV caused the TiO_2 to absorb in the visible region. The valence band (VB) of the $N_{s(O)}$ model is 4.6 eV wide, which is slightly wider than that of pure anatase

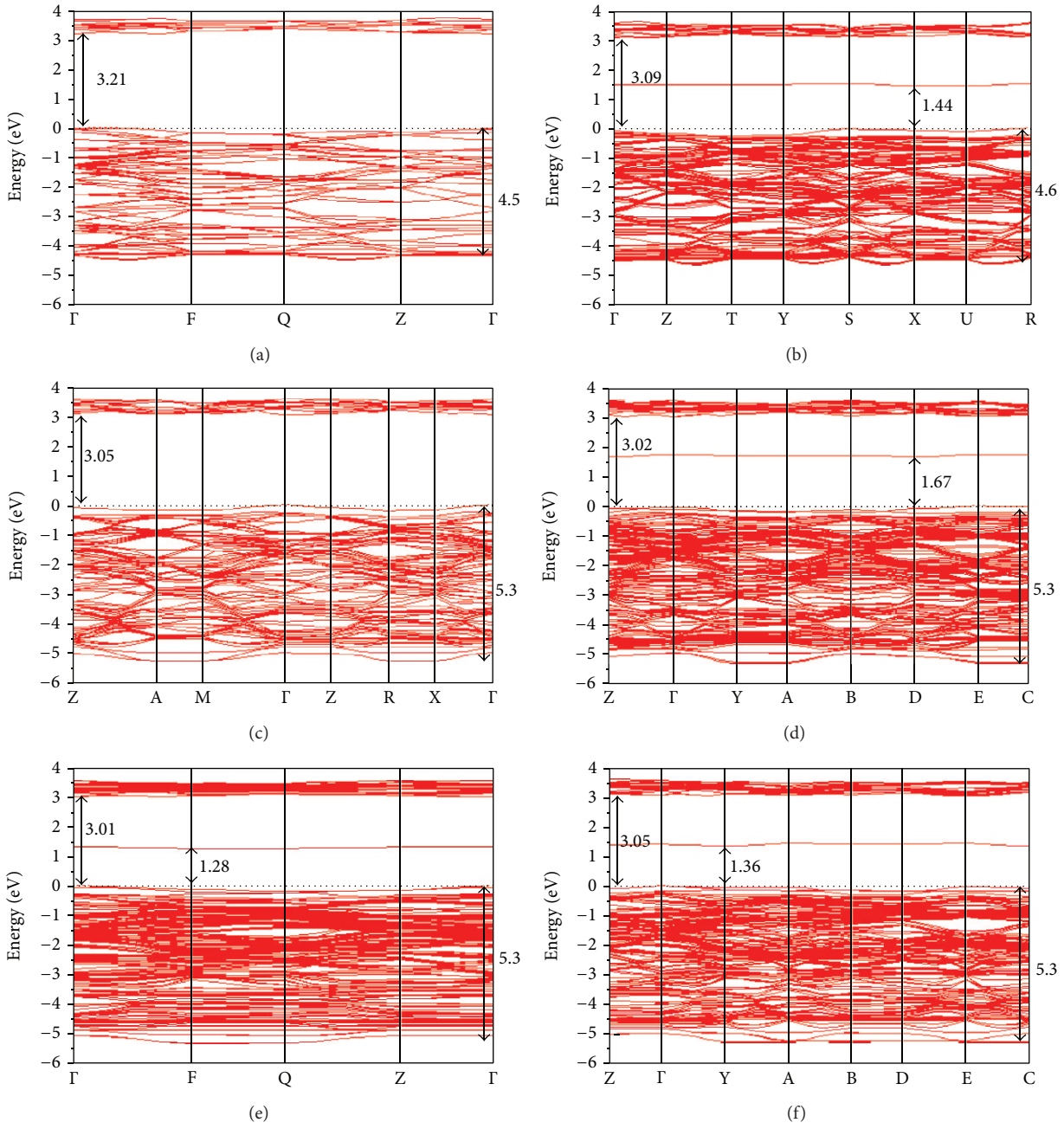

Figure 2: Band structures of N/Si-doped TiO_2 for (a) pure TiO_2, (b) $N_{s(O)}$, (c) $Si_{s(Ti)}$, (d) N/Si-1, (e) N/Si-2, and (f) N/Si-3 models.

TiO_2 (4.5 eV). The bandgap narrowed to 3.05 eV in the $Si_{s(Ti)}$ model (Figure 2(c)). There is no impurity energy level in the forbidden band because the Si and Ti atoms showed equal valencies. It should be noted that the VB of the $Si_{s(Ti)}$ model (5.3 eV) is wider than that of pure anatase TiO_2 and the $N_{s(O)}$ model. A wider VB results in higher photogenerated carrier mobility [20]. The bandgaps were narrowed to 3.01–3.05 eV and the VBs were 5.3 eV wide in the N/Si codoping models (Figures 2(d)–2(f)). All three codoping models showed the impurity energy levels; the N/Si-1 model impurity energy level was the highest.

Figure 3 shows the total density of states (TDOS) and projected density of states (PDOS) near the Fermi level of N/Si-doped TiO_2. They help explain the distribution of each related orbital associated with the constituent elements. The VB mainly consists of the O 2*p* and a few Ti 3*d* and N 2*p* states while the conduction band (CB) comprises the Ti 3*d* and a few O 2*p* states in the $N_{s(O)}$ model (Figure 3(a)). The empty N 2*p* state mainly contributes to the impurity energy levels in the forbidden band. The Si 3*s* electrons appear in the range (−7)–(−6.5) eV in the $Si_{s(Ti)}$ model (Figure 3(b)). The Si 3*p* orbital mainly contributes to the bottom of the VB, thus

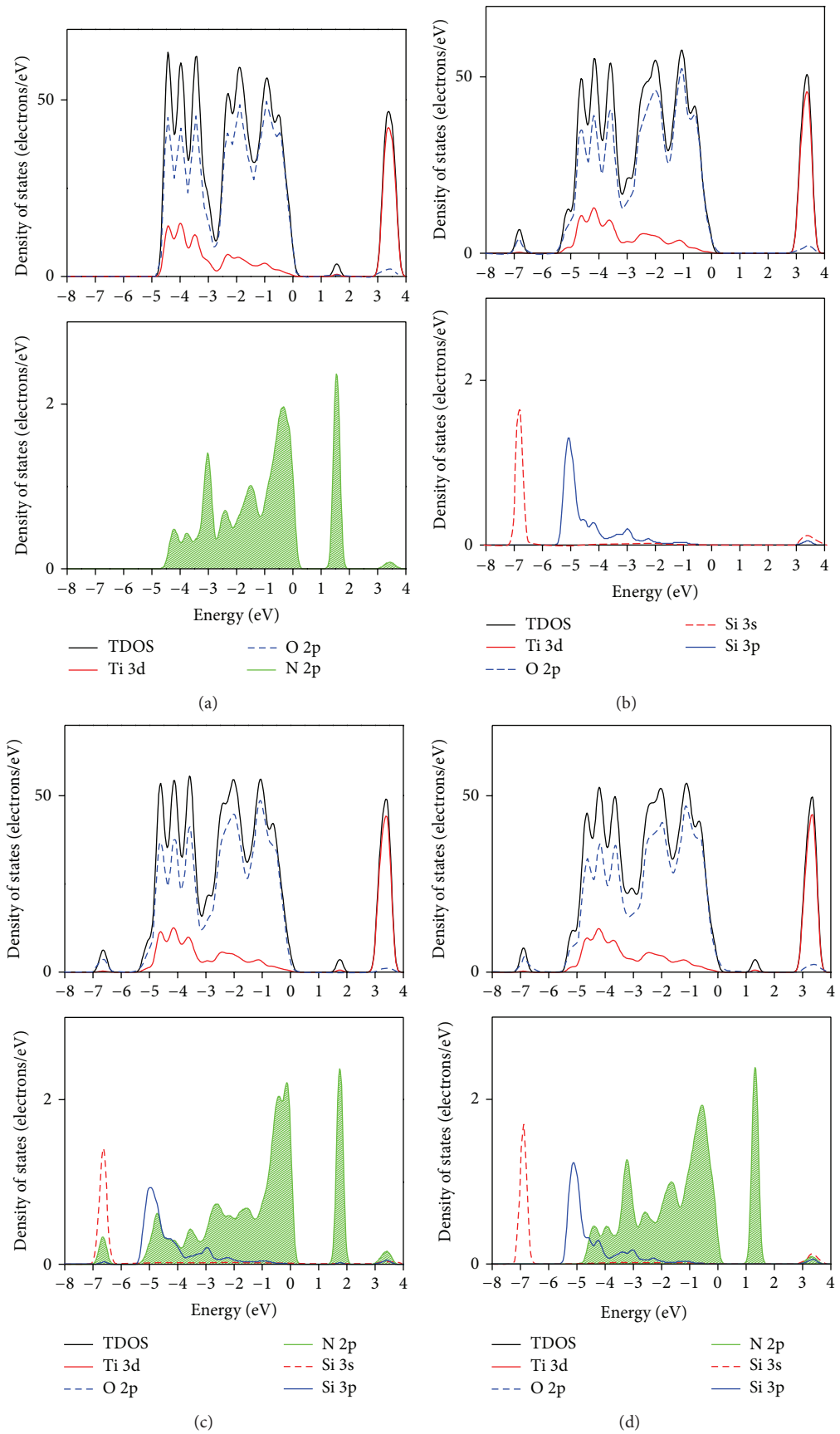

FIGURE 3: Density of states of N/Si-doped TiO_2 for (a) $N_{s(O)}$, (b) $Si_{s(Ti)}$, (c) N/Si-1, and (d) N/Si-2 models.

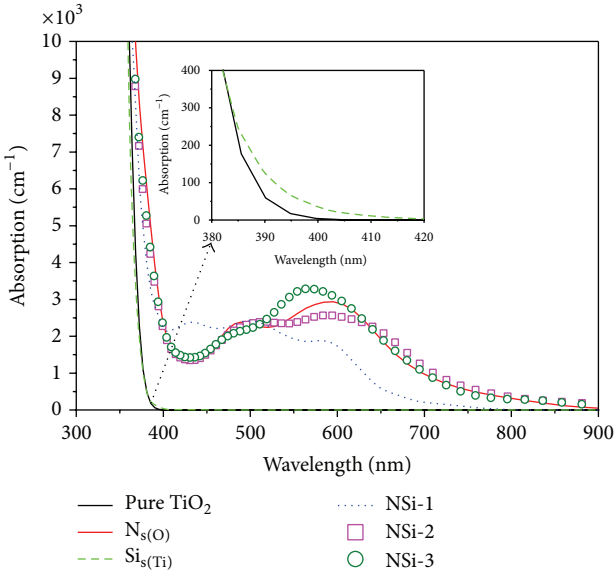

Figure 4: Absorption spectra computed for N/Si-doped TiO_2.

significantly widening it. In the N/Si-1 model (Figure 3(c)), the N 2*p* orbital is hybridized not only with the Si 3*s* orbital in the range (−7)–(−6.5) eV but also with the Si 3*p* orbital in the VB. Therefore, the Si–N bond is more covalent than the Ti–N and Ti–O ones, as mentioned in Section 3.2. In addition, adding Si atoms produced a wider VB and a narrower bandgap in the N/Si-1 model than in the $N_{s(O)}$ one. Figure 3(d) shows the DOS of the N/Si-2 model, which is similar to that of the N/Si-3 one. It should be reemphasized that the Si 3*p* state, not the N 2*p* one, contributes to widening the VB; therefore, the Si 3*p* state played a key role in widening the VB.

3.4. Optical Properties. The optical properties of materials can be obtained using the dielectric function, $\varepsilon(\omega) = \varepsilon_1(\omega) + i\varepsilon_2(\omega)$, whose imaginary part, $\varepsilon_2(\omega)$, is calculated using the following expression [32]:

$$\varepsilon_2 = \frac{2e^2\pi}{\Omega\varepsilon_0} \sum_{k,v,c} \left|\left\langle \varphi_k^c \left| u \cdot r \right| \varphi_k^v \right\rangle\right|^2 \delta\left(E_k^c - E_k^v - \omega\right), \quad (2)$$

where e, Ω, u, ω, and φ_k^v and φ_k^c represent the electronic charge, unit cell volume, vector defining the polarization of the incident electric field, light frequency, and the wave functions of the conduction and VBs, respectively. Kramers-Kronig relations can be used to calculate the real part of the dielectric function, $\varepsilon_1(\omega)$, from $\varepsilon_2(\omega)$. The absorption coefficient, $\alpha(\omega)$, can be obtained from $\varepsilon_1(\omega)$ and $\varepsilon_2(\omega)$.

Figure 4 shows the absorption spectra computed for the N/Si-doped TiO_2. The pure anatase TiO_2 did not show any absorption in the visible region because it shows a wide bandgap of 3.21 eV. Doping the TiO_2 with Si narrowed the bandgap, thereby redshifting the intrinsic absorption edge toward higher wavelengths (Figure 4 inset). The N-doped TiO_2 showed a redshifted intrinsic absorption edge due to the band gap narrowing and the absorption had extended into the visible and infrared (IR) regions, owing also to the N 2p impurity energy level that occurs in the forbidden band mentioned previously in Section 3.3. The forbidden band contained the N 2*p* impurity energy level in all three N/Si codoping models. Therefore, the codoping models exhibited stronger absorption than the pure anatase or Si-doped TiO_2 in the visible region, thereby enhancing photocatalytic activity. It should be noted that the N/Si-1 model shows the stablest structure of the three codoping models and exhibits the strongest absorption between 400 and 500 nm, which is consistent with the previously reported experimental results [17, 18].

4. Conclusions

First principles calculations were performed to study the optimized structure, Mulliken population, electronic structure, and optical properties of N/Si-codoped TiO_2 models. The N/Si-1 model exhibited the stablest structure, whose bond lengths are arranged in descending order as follows: Ti–N > Ti–O > Si–N > Si–O. The bandgaps of the N/Si codoping models were narrowed to 3.01–3.05 eV, and the VBs were widened to 5.3 eV; the Si 3*p* orbital played a key role in extending VB width. All three N/Si codoping models showed the N-induced impurity energy level in the forbidden band; therefore, these models exhibited stronger absorption than the pure anatase TiO_2 and the monodoped models in the visible region and thus showed enhanced photocatalytic activity. According to our theoretical calculations, the bandgap narrowing, VB widening, and impurity energy level in the forbidden band all aid in improving the photocatalytic activity of N/Si-codoped TiO_2.

Conflict of Interests

The authors declare that there is no conflict of interests regarding the publication of this paper.

Acknowledgments

The authors are grateful for the support of the National Science Council in Taiwan (NSC 102-2221-E-131-008). The authors also acknowledge the National Center for High-Performance Computing for computer time and the use of its facilities.

References

[1] A. Fujishima and K. Honda, "Electrochemical photolysis of water at a semiconductor electrode," *Nature*, vol. 238, no. 5358, pp. 37–38, 1972.

[2] Y. K. Du, Y. Q. Gan, P. Yang, F. Zhao, N. P. Hua, and L. Jiang, "Improvement in the heat-induced hydrophilicity of TiO_2 thin films by doping Mo(VI) ions," *Thin Solid Films*, vol. 491, no. 1-2, pp. 133–136, 2005.

[3] M. Subramanian, S. Vijayalakshmi, S. Venkataraj, and R. Jayavel, "Effect of cobalt doping on the structural and optical properties of TiO_2 films prepared by sol-gel process," *Thin Solid Films*, vol. 516, no. 12, pp. 3776–3782, 2008.

[4] M. Zhou, J. Zhang, B. Cheng, and H. Yu, "Enhancement of visible-light photocatalytic activity of mesoporous Au-TiO_2 nanocomposites by surface plasmon resonance," *International Journal of Photoenergy*, vol. 2012, Article ID 532843, 10 pages, 2012.

[5] R. Asahi, T. Morikawa, T. Ohwaki, K. Aoki, and Y. Taga, "Visible-light photocatalysis in nitrogen-doped titanium oxides," *Science*, vol. 293, no. 5528, pp. 269–271, 2001.

[6] H.-C. Wu, S.-W. Lin, and J.-S. Wu, "Effects of nitrogen concentration on N-doped anatase TiO_2: density functional theory and Hubbard U analysis," *Journal of Alloys and Compounds*, vol. 522, pp. 46–50, 2012.

[7] J. Qian, G. Cui, M. Jing, Y. Wang, M. Zhang, and J. Yang, "Hydrothermal synthesis of nitrogen-doped titanium dioxide and evaluation of its visible light photocatalytic activity," *International Journal of Photoenergy*, vol. 2012, Article ID 198497, 6 pages, 2012.

[8] H. Fu, G. Shang, S. Yang, and T. Xu, "Mechanistic study of visible-light-induced photodegradation of 4-chlorophenol by $TiO_{2-x}N_x$ with low nitrogen concentration," *International Journal of Photoenergy*, vol. 2012, Article ID 759306, 9 pages, 2012.

[9] M.-C. Wang, H.-J. Lin, C.-H. Wang, and H.-C. Wu, "Effects of annealing temperature on the photocatalytic activity of N-doped TiO_2 thin films," *Ceramics International*, vol. 38, no. 1, pp. 195–200, 2012.

[10] X. Yan, J. He, D. G. Evans, X. Duan, and Y. Zhu, "Preparation, characterization and photocatalytic activity of Si-doped and rare earth-doped TiO_2 from mesoporous precursors," *Applied Catalysis B: Environmental*, vol. 55, no. 4, pp. 243–252, 2005.

[11] R. Jin, Z. Wu, Y. Liu, B. Jiang, and H. Wang, "Photocatalytic reduction of NO with NH3 using Si-doped TiO_2 prepared by hydrothermal method," *Journal of Hazardous Materials*, vol. 161, no. 1, pp. 42–48, 2009.

[12] M. Sun, X. Zhang, J. Li, X. Cui, D. Sun, and Y. Lin, "Thermal formation of silicon-doped TiO_2 thin films with enhanced visible light photoelectrochemical response," *Electrochemistry Communications*, vol. 16, no. 1, pp. 26–29, 2012.

[13] S. Iwamoto, S. Iwamoto, M. Inoue, H. Yoshida, T. Tanaka, and K. Kagawa, "XANES and XPS study of silica-modified titanias prepared by the glycothermal method," *Chemistry of Materials*, vol. 17, no. 3, pp. 650–655, 2005.

[14] Y. Zhang, X. Li, D. Chen, N. Ma, X. Hua, and H. Wang, "Si doping effects on the photocatalytic activity of TiO_2 nanotubes film prepared by an anodization process," *Scripta Materialia*, vol. 60, no. 7, pp. 543–546, 2009.

[15] Y. Lv, L. Yu, H. Huang, H. Liu, and Y. Feng, "Preparation, characterization of P-doped TiO_2 nanoparticles and their excellent photocatalystic properties under the solar light irradiation," *Journal of Alloys and Compounds*, vol. 488, no. 1, pp. 314–319, 2009.

[16] T. Umebayashi, T. Yamaki, H. Itoh, and K. Asai, "Band gap narrowing of titanium dioxide by sulfur doping," *Applied Physics Letters*, vol. 81, no. 3, pp. 454–456, 2002.

[17] H. Ozaki, S. Iwamoto, and M. Inoue, "Enhanced visible light sensitivity of nitrogen-doped nanocrystalline si-modified titania prepared by the glycothermal method," *Chemistry Letters*, vol. 34, no. 8, pp. 1082–1083, 2005.

[18] H. Ozaki, S. Iwamoto, and M. Inoue, "Effects of amount of Si addition and annealing treatment on the photocatalytic activities of N- and Si-codoped titanias under visible-light irradiation," *Industrial and Engineering Chemistry Research*, vol. 47, no. 7, pp. 2287–2293, 2008.

[19] Y. D. Hou, X. C. Wang, L. Wu et al., "N-Doped SiO_2/TiO_2 mesoporous nanoparticles with enhanced photocatalytic activity under visible-light irradiation," *Chemosphere*, vol. 72, no. 3, pp. 414–421, 2008.

[20] W. Shi, Q. Chen, Y. Xu, D. Wu, and C. Huo, "A first-principles calculation on the electronic properties of Si/N-codoped TiO_2," *Applied Surface Science*, vol. 257, no. 7, pp. 3000–3006, 2011.

[21] R. Long and N. J. English, "Band gap engineering of (N, Si)-codoped TiO_2 from hybrid density functional theory calculations," *New Journal of Physics*, vol. 14, Article ID 053007, 11 pages, 2012.

[22] G. Shao, "Red shift in manganese- and iron-doped TiO_2: a dft+u analysis," *Journal of Physical Chemistry C*, vol. 113, no. 16, pp. 6800–6808, 2009.

[23] X. Ma, B. Lu, D. Li, R. Shi, C. Pan, and Y. Zhu, "Origin of photocatalytic activation of silver orthophosphate from first-principles," *Journal of Physical Chemistry C*, vol. 115, no. 11, pp. 4680–4687, 2011.

[24] H. C. Wu, Y. S. Lin, and S. W. Lin, "Mechanisms of visible light photocatalysis in N-doped anatase TiO_2 with oxygen vacancies from GGA+U calculations," *International Journal of Photoenergy*, vol. 2013, Article ID 289328, 7 pages, 2013.

[25] H. C. Wu, Y. C. Peng, and T. P. Shen, "Electronic and optical properties of substitutional and interstitial si-doped ZnO," *Materials*, vol. 5, no. 11, pp. 2088–2100, 2012.

[26] M. D. Segall, P. J. D. Lindan, M. J. Probert et al., "First-principles simulation: ideas, illustrations and the CASTEP code," *Journal of Physics Condensed Matter*, vol. 14, no. 11, pp. 2717–2744, 2002.

[27] D. Vanderbilt, "Soft self-consistent pseudopotentials in a generalized eigenvalue formalism," *Physical Review B*, vol. 41, no. 11, pp. 7892–7895, 1990.

[28] H. J. Monkhorst and J. D. Pack, "Special points for Brillouin-zone integrations," *Physical Review B*, vol. 13, no. 12, pp. 5188–5192, 1976.

[29] Z. Zhao and Q. Liu, "Mechanism of higher photocatalytic activity of anatase TiO_2 doped with nitrogen under visible-light irradiation from density functional theory calculation," *Journal of Physics D: Applied Physics*, vol. 41, no. 2, Article ID 025105, 10 pages, 2008.

[30] D. R. Lide, Ed., *CRC Handbook of Chemistry and Physics*, Taylor & Francis, Boca Raton, Fla, USA, 2006.

[31] R. D. Shannon, "Revised effective ionic radii and systematic studies of interatomic distances in halides and chalcogenides," *Acta Crystallographica*, vol. 32, pp. 751–767, 1976.

[32] R. Chowdhury, S. Adhikari, and P. Rees, "Optical properties of silicon doped ZnO," *Physica B: Condensed Matter*, vol. 405, no. 23, pp. 4763–4767, 2010.